NRL Report 7910

A Fracture Mechanics and Fractographic Study of Fatigue-Crack Propagation Resistance in 17-4 PH Stainless Steels

T. W. CROOKER
Engineering Materials Division
Naval Research Laboratory

D. F. HASSON
Department of Mechanical Engineering
U. S. Naval Academy

G. R. YODER
Engineering Materials Division
Naval Research Laboratory

July 17, 1975

NAVAL RESEARCH LABORATORY
Washington, D.C.

REPORT DOCUMENTATION PAGE		READ INSTRUCTIONS BEFORE COMPLETING FORM
1. REPORT NUMBER NRL Report 7910	2. GOVT ACCESSION NO.	3. RECIPIENT'S CATALOG NUMBER
4. TITLE (and Subtitle) A FRACTURE MECHANICS AND FRACTOGRAPHIC STUDY OF FATIGUE CRACK PROPAGATION RESISTANCE IN 17-4 PH STAINLESS STEELS		5. TYPE OF REPORT & PERIOD COVERED Final report on one phase of a continuing NRL problem. 6. PERFORMING ORG. REPORT NUMBER
7. AUTHOR(s) T. W. Crooker, D. F. Hasson, and G. R. Yoder		8. CONTRACT OR GRANT NUMBER(s)
9. PERFORMING ORGANIZATION NAME AND ADDRESS Naval Research Laboratory Washington, D.C. 20375		10. PROGRAM ELEMENT, PROJECT, TASK AREA & WORK UNIT NUMBERS NRL Problem M01-24 Project RR 022-01-46-5431
11. CONTROLLING OFFICE NAME AND ADDRESS Department of the Navy Office of Naval Research Arlington, Va. 22217		12. REPORT DATE July 17, 1975 13. NUMBER OF PAGES 21
14. MONITORING AGENCY NAME & ADDRESS(if different from Controlling Office)		15. SECURITY CLASS. (of this report) Unclassified 15a. DECLASSIFICATION/DOWNGRADING SCHEDULE

16. DISTRIBUTION STATEMENT (of this Report)

Approved for public release; distribution unlimited.

17. DISTRIBUTION STATEMENT (of the abstract entered in Block 20, if different from Report)

18. SUPPLEMENTARY NOTES

19. KEY WORDS (Continue on reverse side if necessary and identify by block number)

Fatigue crack propagation
Fractography
Fracture mechanics
Stainless steels

20. ABSTRACT (Continue on reverse side if necessary and identify by block number)

A determination of fatigue-crack propagation resistance in heat-treated samples of 17-4 PH stainless steel has been made, together with correlative microscopic observations via electron fractography. Two rolled plates of 1/2-in. thickness were investigated, one vacuum melted (VM) and heat treated to the H1050 condition and the other argon-oxygen melted (AOM) and heat treated to the H1050 and H1150 conditions. Crack-growth rates (da/dN) were obtained in ambient laboratory air as a function of stress-intensity factor range ΔK using single-edge-notched (SEN) tension specimens. The effect of stress ratio R on da/dN was examined; values

(Continued)

20. ABSTRACT (Cont.)

of R = 0.04, 0.40, 0.67, and 0.80 were employed. Microscopic modes of crack propagation determined by electron fractography were utilized to explain differences in macroscopic crack-growth behavior. Both cleavage and microvoid coalescence can appear as modes of cyclic crack propagation in this family of steels, to the detriment of cyclic crack-growth resistance. When cleavage is present, the amount appears to be independent of ΔK over a wide spectrum of ΔK levels. Moreover, the incidence of cleavage (and accelerated cyclic crack propagation rates) increases significantly with ratio R. It was found that the heat treatment can be adjusted to minimize the incidence of cleavage, and that slight variation in alloy processing serves to eliminate cleavage and promote striation formation, while enhancing the fracture toughness.

CONTENTS

A FRACTURE MECHANICS AND FRACTOGRAPHIC STUDY OF FATIGUE CRACK PROPAGATION RESISTANCE IN 17-4 PH STAINLESS STEELS

INTRODUCTION

High-strength precipitation hardening (PH) stainless steels are among the candidate materials for application in new high-performance surface ships. Such sophisticated applications will require a far more comprehensive knowledge of the mechanical characteristics of these materials than presently exists. The study reported here was undertaken to develop basic engineering information on the cyclic crack-growth behavior of 17-4 PH stainless steels. The 17-4 family of PH stainless steels represents a highly complex and incompletely understood alloy system. The mechanical properties of 17-4 PH steels can vary widely, depending upon processing and heat treatment [1, 2]. This investigation resulted in data on and interpretation of cyclic crack growth in samples of 17-4 PH steels of interest for potential application in naval structures. Both macroscopic fracture-mechanics cyclic crack-growth test results and microscopic electron fractography interpretations are presented.

DESCRIPTION OF MATERIALS

Two 1/2-in.-thick rolled plates of 17-4 PH stainless steel were studied, a vacuum-melted (VM) sample in the H1050 condition and an argon-oxygen melted (AOM) sample in the H1050 and H1150 conditions. Chemical compositions of the two plates are given in Table 1. Rough-cut specimen blanks were solution treated at 1900°F for 1 hr. in an

Table 1
Chemical Compositions by Element (wt. pct.)

Melt	Cr	Ni	Cu	C	Mn	P	S	Si	N	Cb	Ta	Co
AOM	15.84	4.26	3.36	0.032	0.32	0.02	0.017	0.60	—	0.22	0.01	—
VM	15.81	4.47	3.34	0.046	0.26	0.02	0.008	0.53	0.016	0.28	0.01	0.04

argon atmosphere, followed by an oil quench. Machined specimens were then aged in an air atmosphere at either 1050 or 1150°F for 4 hr., followed by air cooling. Mechanical properties of the heat-treated materials are shown in Table 2.

The resulting metallographic features are shown in Figs. 1-3. Although no difference in prior austenite grain size is apparent between the VM and AOM plates (Fig. 1), they do

Note: Manuscript submitted May 21, 1975.

exhibit a distinct difference in inclusion populations, as illustrated in Fig. 2. Although both the AOM and VM plates appear to contain similar, relatively small inclusions of uniform distribution (but perhaps of greater density in the VM plate), the AOM plate also contains notable strings of relatively large inclusions. Both plates contain stringers of δ-ferrite, as exhibited in Fig. 3; however, the AOM plate contains more of this phase.

Table 2
Mechanical Properties

Melt	Condition	5/8-in.* DTE (ft-lb)	σys (ksi)	σuts (ksi)	Elongation (%)	Reduction of Area (%)	Hardness R_c
AOM	H1050	110	163.0	170.8	12.5	47.2	36.8
AOM	H1150	125	135.0	148.6	14.2	48.0	32.5
VM	H1050	480	153.6	160.3	16.0	62.0	34.3

*See Ref. 3.

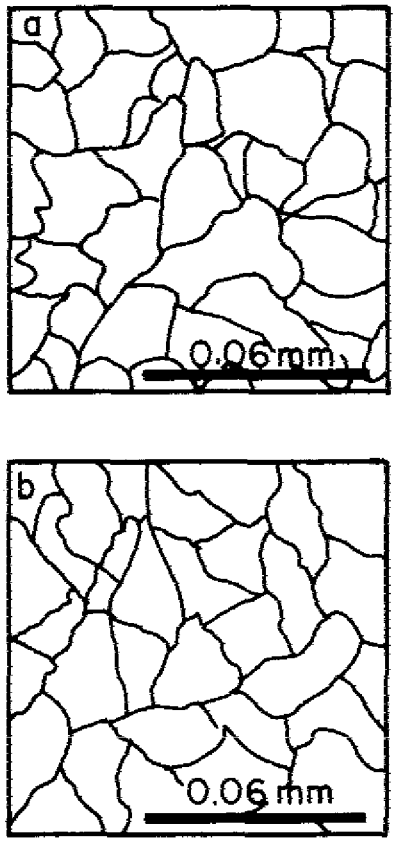

Fig. 1 — Traces of prior austenite grains in (a) AOM plate and (b) VM plate

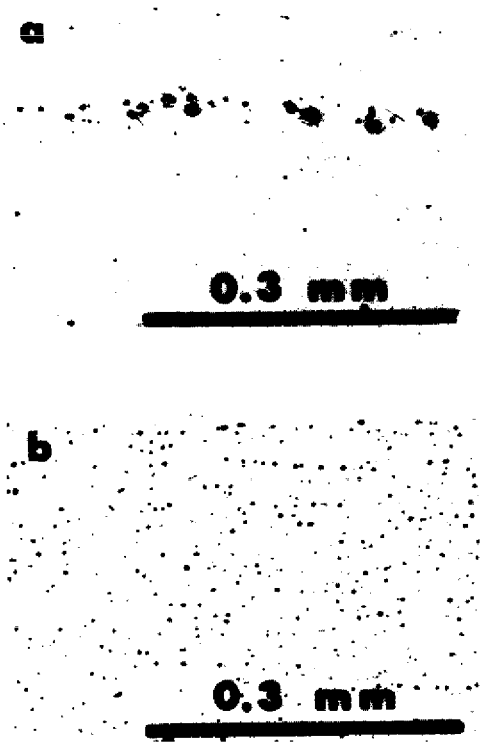

Fig. 2 — Inclusion distributions in (a) AOM-H1150 steel and (b) VM-H1050 steel. As polished.

EXPERIMENTAL PROCEDURES

Fatigue crack growth rate (FCGR) tests were conducted on each of the three materials studied. Single-edge-notch (SEN) tension specimens 0.475-in. thick, shown schematically in Fig. 4a, were employed in the FCGR tests. Crack propagation in these specimens occurred in the T-L orientation [4]. The proportions of these specimens and the stress-intensity formulation utilized in calculating ΔK values were obtained from Ref. 5. Fatigue crack growth rate tests were conducted on a 110-kip capacity closed-loop fatigue machine in ambient laboratory air at a frequency of 5 Hz. Observations of crack length were made optically at approximately 15X using a Gaertner traveling microscope. Specimens of each material were tested at various stress ratios (minimum stress-intensity factor/maximum stress-intensity factor stress = R). Ratios of 0.04, 0.40, 0.67, and 0.80 were studied. Duplicate specimens were tested in each case, and all FCGR curves reported include data from two specimens. One specimen was first tested under constant load, then a second specimen was step-loaded with the load increased incrementally after each 0.100 in. of crack growth.

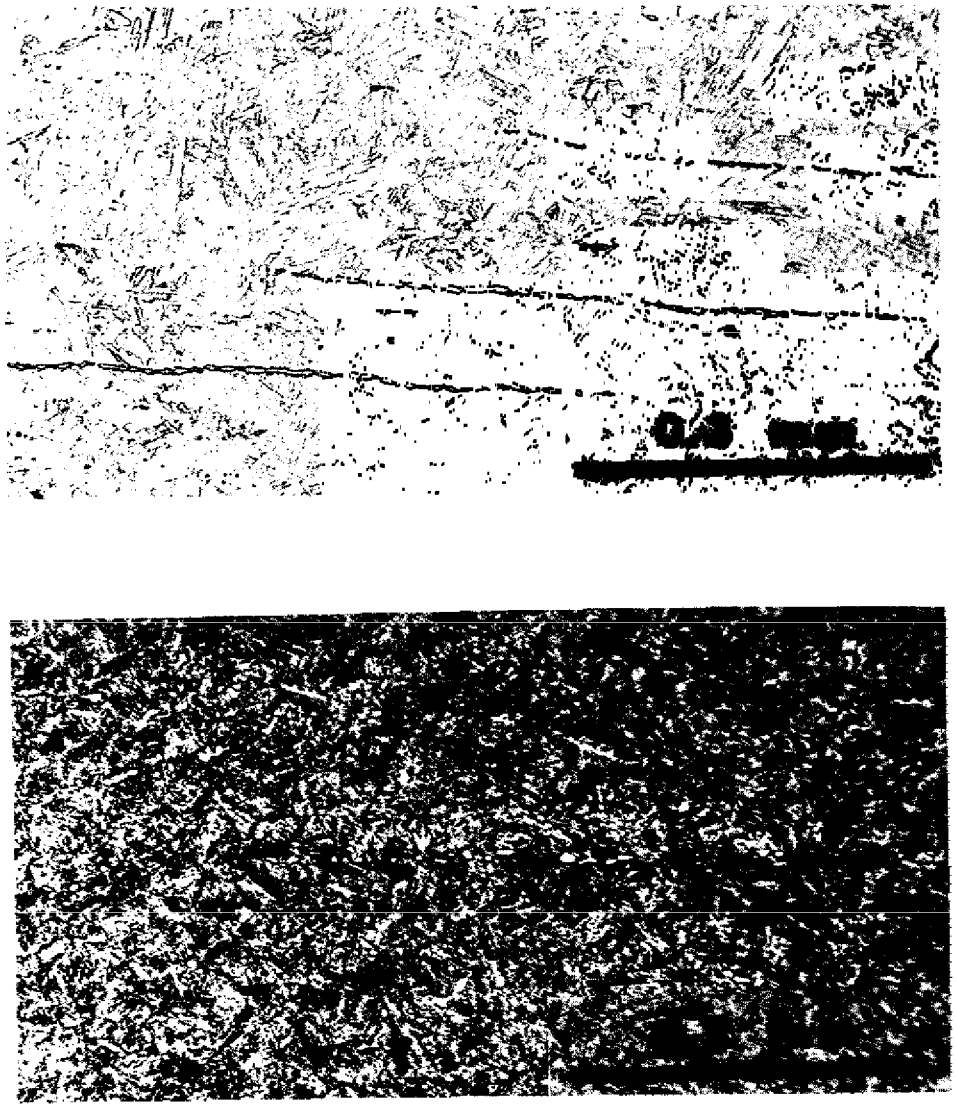

Fig. 3 — Delta ferrite in the (a) AOM-H1050 steel and (b) VM-H1050 steel. Etched with Vilella's reagent.

Tensile tests were conducted on 0.357-in. diameter specimens taken from the SEN specimens following FCGR testing. Fracture-toughness values were obtained from 5/8-in. Dynamic Tear specimens, Fig. 4b, tested at ambient laboratory temperature in accordance with Ref. 3.

Replicas were made to determine the mode of cyclic crack propagation across the spectrum of stress-intensity ranges examined. These replicas were made from cellulose acetate films which were stripped from the fatigue fracture surfaces (at the midthickness

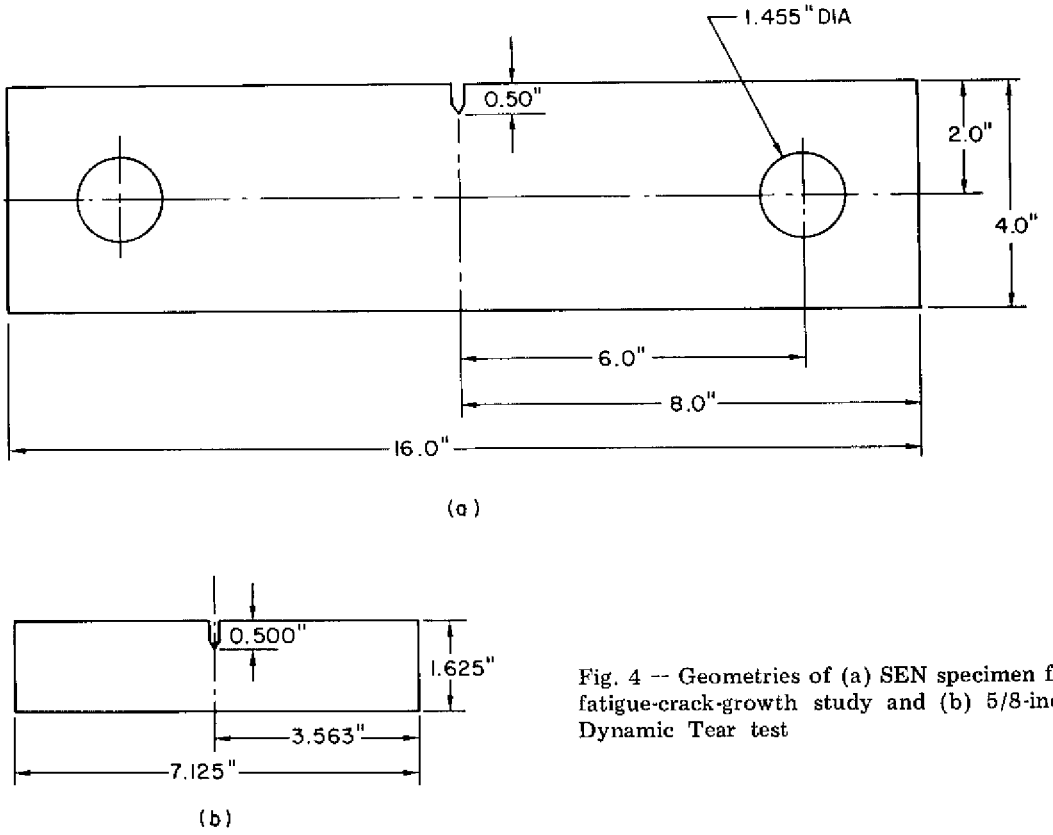

Fig. 4 -- Geometries of (a) SEN specimen for fatigue-crack-growth study and (b) 5/8-inch Dynamic Tear test

positions), shadowed with platinum, and then deposited with a carbon backing. Visual estimates of percentages of the constituent microfracture modes were made by thoroughly examining each replica.

RESULTS

The fracture-mechanics, cyclic crack growth results are presented in Fig. 5a, b, c. These are logarithmic plots of crack growth rate da/dN vs crack-tip stress-intensity factor range ΔK for each of the three materials studied.* In each case, the minimum ΔK values reported were near 10 ksi$\sqrt{\text{in.}}$, and several R values are included. Tests were continued to the maximum stress-intensity level at which optical observation of cyclic crack growth could be maintained for each combination of material and stress ratio studied. Tests were terminated either because of the occurrence of fracture or because of experimental difficulties in monitoring full-slant shear-mode cracks which were known to have irregular crack front shapes. The significant features of these results are the variation in da/dN values shown as a function of material variables (processing and heat treatment) and the varying sensitivities to R. For any given set of values of ΔK and R, da/dN values can vary by as much as a factor of five due to metallurgical effects. Also, for any of the materials studied, da/dN values at any level of ΔK can vary widely in response to variations in R, especially for higher levels of ΔK.

* For tabulations of these data, refer to Appendix A.

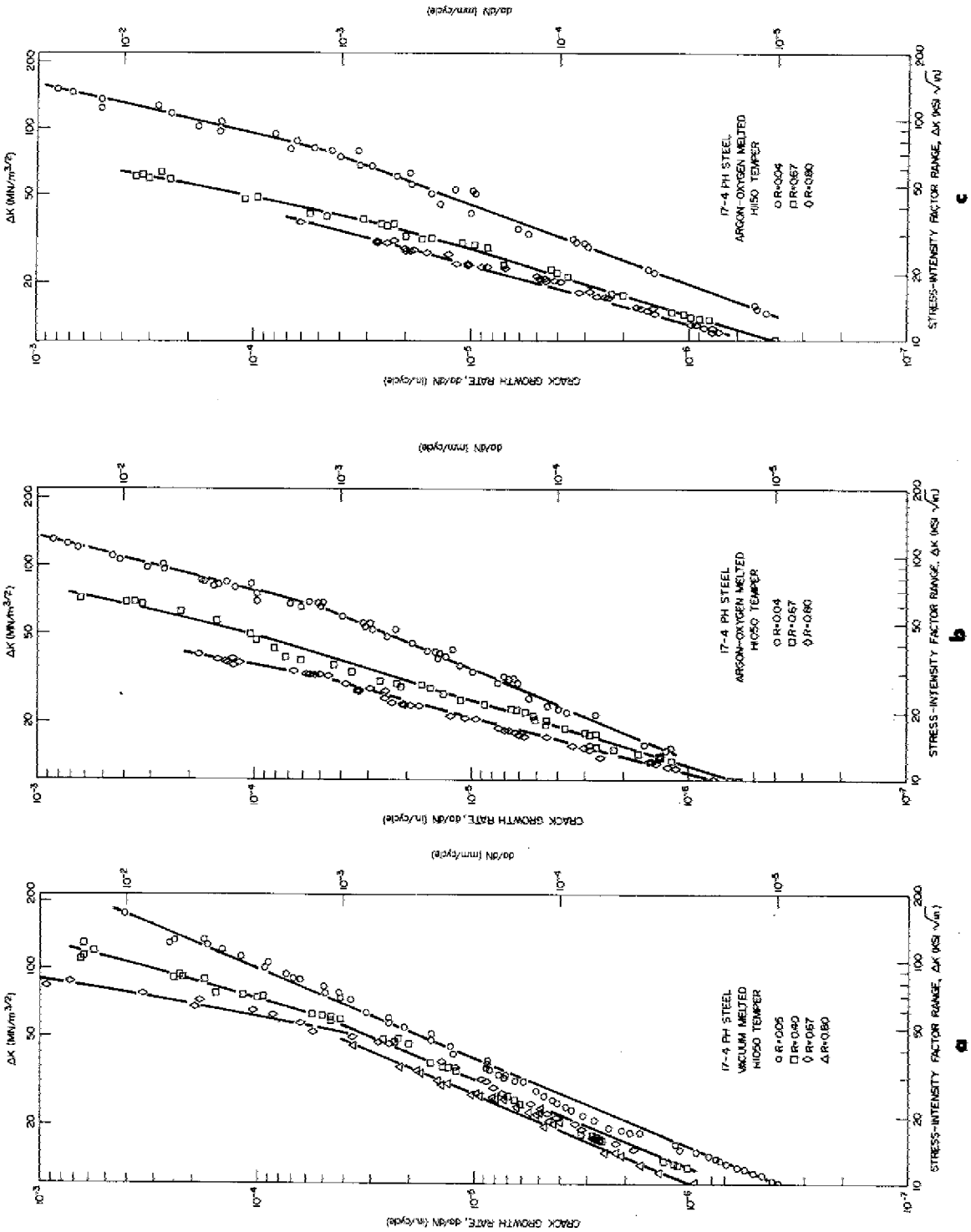

Fig. 5 — Fatigue crack growth data for (a) VM-H1050 steel, (b) AOM-H1050 steel, and (c) AOM-H1150 steel

The DT fracture test results are plotted in Fig. 6, which is a modification of the Ratio Analysis Diagram (RAD) for steels [6]. This cumulative plot of fracture toughness vs yield strength is useful in the present work for comparing the relative strengths and

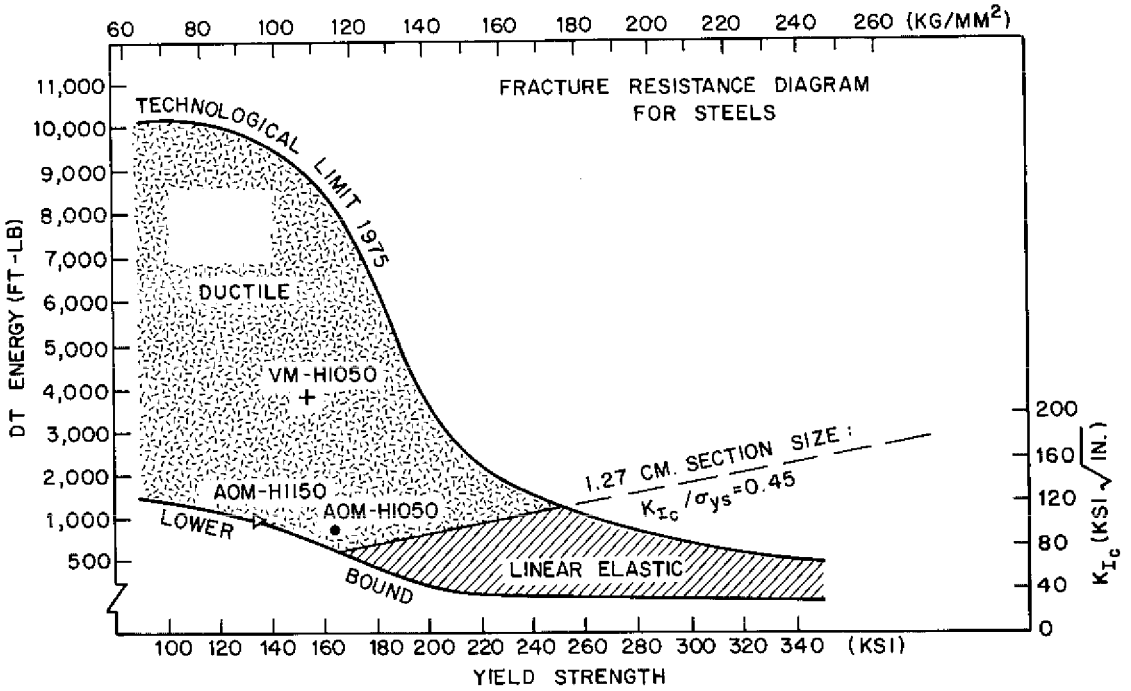

Fig. 6 — Fracture resistance diagram for steels

toughness values of the three materials studied to one another, as well as to the overall range of fracture toughness values measured in extensive prior testing of steels. The results from the 5/8-in. Dynamic Tear (DT) test were plotted in Fig. 6 using procedures outlined in Ref. 7. It can be seen that for the three materials studied, processing exerts a greater influence on toughness than does heat treatment. Both of the AOM materials studied are of low toughness, whereas the VM material exhibited significantly greater toughness.

The principal fractographic results are summarized in Table 3. As outlined in Table 3, a wide range of fracture mechanisms was detected from the fatigue surfaces of the specimens examined, including striations (STR), microvoid coalescence (MVC), and microcleavage (CLE). Since cleavage is a particularly low-energy mode of crack extension and is associated with poor resistance to crack growth, both in fracture and in stress-corrosion cracking, considerable significance is placed on its occurrence under conditions of cyclic crack growth. An example of microcleavage observed in the AOM H1050 material is shown in a stereographic pair of electron fractographs in Fig. 7. It is worth noting that the occurrence of CLE was virtually confined to the AOM H1050 material and its occurrence, along with the associated accelerated crack growth rates, could be suppressed either through processing or heat-treatment variations.

Table 3
Summary of Microfractographic Modes of Fatigue Crack Growth

Material	ΔK(ksi$\sqrt{\text{in.}}$)	R = 0.04	ΔK(ksi$\sqrt{\text{in.}}$)	R = 0.67
AOM-H1050	29	2-3% CLE >95% STR	15	15-20% CLE ~15% MVC 65-70% STR
	49	2-3% CLE 10-15% MVC ~85% STR	26	15-20% CLE ~70% MVC 10-15% STR
	63	2-5% CLE ~15% MVC 80-85% STR	35	15-20% CLE ~75% MVC 5-10% STR
	121	5% CLE 85% MVC 10% STR	55	~1% CLE ~85% MVC 15% STR
AOM-H1150	30	100% STR	17	1-2% CLE ~20% MVC 75-80% STR
	70	25% MVC 75% STR	24	1-2% CLE ~20% MVC 75-80% STR
	148	100% MVC	30	1-2% CLE ~40% MVC 60% STR
	—*	—	47	1% CLE ~50% MVC 50% STR
VM-H1050	24	100% STR	23	~1% CLE 5% MVC ~95% STR
	52	100% STR	35	~1% CLE 5-10% MVC 90-95% STR
	100	15% MVC 85% STR	49	~1% CLE 15% MVC ~85% STR
	--	—	80	~1% CLE ~95% MVC 5% STR

*Dashes indicate no further observations.

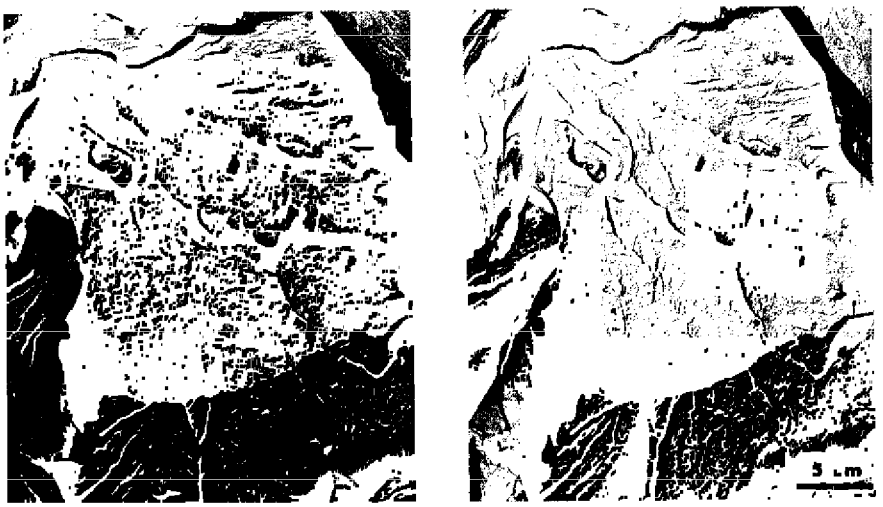

Fig. 7 — Microcleavage mode of fatigue crack growth in the AOM-H1050 steel, $R = 0.67$, $\Delta K = 35 \text{ksi}\sqrt{\text{in}}$. Steroscopic pair of replica electron fractographs.

DISCUSSION

Fracture Results

The fracture results, which indicate a very distinct beneficial effect of vacuum melting, are in excellent agreement with the much more extensive fracture studies on 17-4 PH steels conducted by Judy et al. [1]. Beneficial purity effects on fracture toughness resulting from vacuum melting are well recognized in steels and are the principal factor in determining metal quality "corridors" on the RAD [6]. It should be pointed out that the AOM material does not appear amenable to significant improvement in fracture toughness through variation in heat treatment and falls among the least fracture-resistant steels available at the respective yield-strength levels studied [1].

Cyclic Crack Growth Results

Several investigations have shown that cyclic crack growth, as measured in terms of da/dN values as a function of ΔK, is remarkably invariant in a broad selection of steels (principally martensitic), ranging in yield strength from intermediate to ultrahigh levels [8-10]. Conversely, other investigators have shown significant and systematic variations in da/dN values in similar types of steels which can be related to macromechanical properties or heat treatment [2,11-13]. However, these previous investigations of cyclic crack growth in steels

have tended, for the most part, to limit the loading conditions to R values near zero (zero-to-tension), and to make relatively few fractographic observations as a means of explaining variations (or the lack thereof) in behavior. Thus, an incomplete and somewhat confusing picture of cyclic crack growth behavior in high-strength steels exists.

Recent investigations conducted in Great Britain have begun to remedy this void in our knowledge of cyclic crack-growth behavior of metallic materials [14-18]. The findings of these separate investigations largely support the observations of the authors' study of 17-4 PH steels.

The da/dN vs ΔK results shown in Fig. 5 indicate distinct differences in the cyclic crack-growth characteristics of the three 17-4 PH steels studied. Several salient observations are as follows: First, for virtually any combination of ΔK and R, the H1050 VM material exhibits lower crack growth rates than does the H1050 AOM material. This can be regarded as a beneficial purity effect and is in agreement with the findings of Evans et al. [14]. Second, heat treating the AOM material to the lower yield-strength H1150 temper significantly improves the cyclic crack-growth resistance at the low R value (0.04), as compared to the H1050 AOM material at the same R value, and results in da/dN values comparable to the VM material despite significant differences in fracture toughness between the AOM H1150 and VM H1050 materials. However, at higher R values, the lower toughness H1150 AOM material develops significantly higher da/dN values than does the H1050 VM material. This finding is in general agreement with the results of Rack and Kalish [2]. Third, each material exhibits a significant dependence of da/dN on R, which is most pronounced in the lower toughness materials; and, this R-factor dependence diminishes with decreasing ΔK. In fact, there is a tendency for convergence of nearly all the curves at ΔK levels near 10 ksi$\sqrt{\text{in.}}$. These observations agree, at least in part, with the findings of most of the British investigations cited in Refs. 14-18.

In recent years, numerous FCGR laws which account for stress-ratio effects have been formulated. However, attempts to normalize each of the sets of data shown in Figs. 5a, b, and c into a unified format were unsuccessful. Obviously, in a situation where metallurgical factors exert such a pronounced effect on cyclic crack growth behavior, no single law based on continuum mechanics principles will successfully describe such varied behavior. Rather, an understanding of micromechanistic events is necessary.

Fractographic Results

As shown above, both the VM and AOM steels in the H1150 condition exhibit a growth rate dependence on R, although the dependence is greater in the case of the AOM plate. And for a given value of R, the crack propagation rate is higher for the AOM plate. Electron fractography reveals that this difference in behavior between the two plates correlates with the propensity toward cleavage as a mode of cyclic crack extension. For example, at R = 0.04, the AOM-H1050 steel exhibits 2-5% CLE for ΔK levels from 29 to 121 ksi$\sqrt{\text{in.}}$. At R = 0.67, however, much more CLE appears, viz, a constant level of 15-20% for ΔK ranges of 15 to 35 ksi$\sqrt{\text{in.}}$. On the other hand, the VM-H1050 steel exhibits no cleavage at R = 0.04, over the whole spectrum of ΔK levels examined; at R = 0.67, just a trace of CLE (1%) appears at ΔK levels from 23 to 80 ksi$\sqrt{\text{in.}}$. Thus, the incidence

of CLE appears to coincide with the poorer crack-growth-rate resistance of the AOM plate. The greater propensity toward cleavage in the AOM plate might be related to the greater percentage of δ-ferrite in the microstructure.

When AOM steel was aged at a higher temperature to obtain the H1150 condition, cleavage was completely suppressed as a mode of crack extension, for R = 0.04, and the crack growth rates were reduced significantly to levels less than or equal to those for the VM steel in the H1050 condition. This improvement might be related to the increased formation of reverted austenite in going from the H1050 to the H1150 condition in the AOM steel, or to the alteration of some feature of the precipitation-hardening mechanism, e.g., the magnitude of the coherency strains. For cyclic crack growth at R = 0.67, a trace of CLE (1-2%) did appear at all ΔK levels examined, from 17 to 47 ksi$\sqrt{\text{in.}}$, just as it did in the case of the VM steel in the H1050 condition.

While microcleavage is not uncommon as a mode of cyclic crack propagation in alloys of various families, the nature of its occurrence in the present case is enigmatic in one respect, viz, that the percent CLE appears to be independent of ΔK over wide ranges of ΔK. This finding contrasts with that for the H900 condition of a 17-4 PH steel studied by Rack and Kalish [2], who reported that percent CLE increased with ΔK. While it has been reported for other alloys that the percent CLE decreases with increased ΔK [19,20], this is the first known instance where the percent CLE appears independent of ΔK, for a given value of R. Much further work may be required for a full understanding of this behavior.

SUMMARY

Fatigue crack propagation rates da/dN in ambient laboratory air have been obtained as a function of stress-intensity factor range ΔK for an argon-oxygen melted steel in the H1050 and H1150 conditons, and for a vacuum-melted steel in the H1050 condition. These growth rates were determined for stress-intensity factor ratios R = 0.04, 0.40, 0.67, and 0.80. Modes of crack extension were determined by electron fractography to elucidate differences in crack-growth-rate behavior. Cleavage appears as a mode of cyclic crack propagation in this family of steels, to the detriment of cyclic crack-growth resistance. In particular, it was found that (a) the amount of cleavage appears to be independent of ΔK over a wide spectrum of ΔK levels, (b) the amount of cleavage (as well as the associated cyclic crack propagation rates) increases significantly with R, (c) heat treatment can be adjusted to minimize the appearance of cleavage, and (d) slight variations in alloy processing serve to eliminate cleavage.

ACKNOWLEDGMENTS

The authors wish to thank Mrs. S. M. McCoy, Mr. G. W. Jackson, and Mr. W. E. King, Jr., for their assitance in conducting the experimental phases of this study. The study was supported by the Naval Materiel Command and the Office of Naval Research.

REFERENCES

1. R. W. Judy, Jr., C. T. Fujii, and R. J. Goode, "Properties of 17-4 PH Steels," NRL Report 7639, Dec. 18, 1973.

2. H. J. Rack and D. Kalish, "The Strength, Fracture Toughness, and Low Cycle Fatigue Behavior of 17-4 PH Stainless Steel," Met. Trans. 5, 1595-1605. (July 1974).

3. MIL-STD-1601 (SHIPS), "Method for 5/8 Inch Dynamic Tear Testing of Metallic Materials," 8 May 1973.

4. R. J. Goode, "Indentification of Fracture Plane Orientation," Mater. Res. Stand. **12**, No. 9, 31-32 (Sept. 1972).

5. W. F. Brown, Jr., and J. E. Srawley, *Plane Strain Crack Toughness Testing of High Strength Metallic Materials*, ASTM STP 410, American Society for Testing and Materials, 1967.

6. W. S. Pellini, "Integration of Analytical Procedures for Fracture-Safe Design of Metal Structures," NRL Report 7251, Mar. 26, 1971.

7. R. W. Judy, Jr., and R. J. Goode, "Ductile Fracture Equation for High-Strength Structural Metals," NRL Report 7557, Apr. 3, 1973.

8. R. C. Bates and W. G. Clark, Jr., "Fractography and Fracture Mechanics," ASM Trans. **62**, No. 2, 380-389 (June 1969).

9. J. M. Barsom, E. J. Imhof, and S. T. Rolfe, "Fatigue-Crack Propagation in High Yield-Strength Steels," Eng. Fracture Mech. **2**, No. 4, 301-317 June 1971.

10. T. W. Crooker, "Fatigue and Corrosion-Fatigue Crack Propagation in Intermediate-Strength Aluminum Alloys," ASME Trans. **95**, Ser. H, No. 3, 150-156 (July 1973).

11. G. A. Miller, "The Dependence of Fatigue-Crack Growth Rate on the Stress Intensity Factor and the Mechanical Properties of Some High-Strength Steels," ASM Trans. **61**, No. 3, 442-448 (Sept. 1968).

12. A. A. Anctil and E. B. Kula, *Effect of Environment and Load History on Fatigue Life*, ASTM STP 462, American Society for Testing and Materials, 1970, pp. 297-317.

13. J. F. Throop and G. A. Miller, "Optimum Fatigue Crack Resistance," *Achievement of High Fatigue Resistance in Metals and Alloys*, ASTM STP 467, American Society for Testing and Materials, 1970, pp. 154-168.

14. P. R. V. Evans, N. B. Owen, and B. E. Hopkins, "The Effect of Purity on Fatigue Crack Growth in a High-Strength Steel," Eng. Fracture Mech. **3**, No. 4, 463-473 (Dec. 1971).

15. S. Pearson, "The Effect of Mean Stress of Fatigue Crack Propagation in Half-Inch (12.7mm) Thick Specimens of Aluminium Alloys of High and Low Fracture Toughness," Eng. Fracture Mech. 4, No. 1, 9-24 (Mar. 1972).

16. C. E. Richards and T. C. Lindley, "The Influence of Stress Intensity and Microstructure on Fatigue Crack Propagation in Ferritic Materials," Eng. Fracture Mech. 4, No. 4, 951-978 (Dec. 1972).

17. R. O. Ritchie and J. F. Knott, "Mechanisms of Fatigue Crack Growth in Low Alloy Steel," Acta Met. 21, 639-648 (May 1973).

18. R. O. Ritchie and J. F. Knott, "Micro Cleavage Cracking During Fatigue Crack Propagation in Low Strength Steel," Mater. Sci. Eng. 14, No. 12, 7-14 (1974).

19. A Yuen, S. W. Hopkins, G. R. Leverant, and C. A. Rau, "Correlations between Fracture Surface Appearance and Fracture Mechanics Parameters for Stage II Fatigue Crack Propagation in Ti-6A1-4V," Met. Trans. 5, No. 8, 1833-42 (1974).

20. K. R. L. Thompson and J. V. Craig, "Fatigue Crack Growth Along Cleavage Planes in an Aluminum Alloy," Met. Trans. 1, 1047-49, (1970).

Appendix A

FATIGUE CRACK GROWTH DATA FOR 17-4 PH STAINLESS STEEL

This appendix contains a tabulation of the fatigue crack growth rate (da/dN) vs stress-intensity factor range (ΔK) data plotted in Figs. 5a, b, and c.

Table A1
Steel: AOM-H1050
Specimen No.: U46-WR1
R: 0.04

ΔK (ksi$\sqrt{\text{in.}}$)	da/dN (in./cycle)
20.9	3.98×10^{-6}
23.2	5.44
27.0	7.55
30.2	9.87
32.4	1.12×10^{-5}
35.1	1.48
38.3	1.58
41.5	1.88
44.8	2.46
47.8	2.82
50.7	3.23
54.7	3.93
58.7	5.08
68.4	9.76
74.0	1.24×10^{-4}
79.4	1.78
86.4	2.63
95.8	4.55

Table A2
Steel: AOM-H1050
Specimen No.: U46-WR4
R: 0.04

ΔK (ksi$\sqrt{\text{in.}}$)	da/dN (in./cycle)
13.7	1.28×10^{-6}
14.1	1.20
14.5	1.59
19.9	2.65
20.4	3.60
21.0	3.80
21.5	4.48
27.9	6.05
28.3	6.65
28.7	6.95
29.1	6.30
29.5	7.05
36.7	1.32×10^{-5}
37.3	1.39
38.4	1.45
39.0	1.21
47.5	2.25
49.2	3.09
50.2	3.18
51.0	2.98
60.5	4.90
61.3	5.15
62.0	6.90
62.7	4.80
63.3	5.65
74.2	1.53×10^{-4}
75.2	1.44
76.1	1.07
77.0	1.35
78.1	1.70
89.5	3.11
92.1	2.63
95.3	4.13
110	6.58
114	7.32
118	8.58

Table A3
Steel: AOM-H1050
Specimen No.: U46-WR2
R: 0.67

ΔK (ksi$\sqrt{\text{in.}}$)	da/dN (in./cycle)
16.3	2.71×10^{-6}
17.1	3.70
17.9	4.50
18.8	5.09
20.0	5.60
21.1	6.53
22.1	8.68
23.3	1.13×10^{-5}
24.8	1.34
26.3	2.12
27.8	2.68
30.4	3.58
33.2	4.32
35.3	7.19
38.7	8.19
43.1	9.78
47.5	1.07×10^{-4}
51.7	1.48
56.8	2.22
63.6	3.88

Table A4
Steel: AOM-H1050
Specimen No.: U46-WR3
R: 0.67

ΔK (ksi$\sqrt{\text{in.}}$)	da/dN (in./cycle)
10.2	5.90×10^{-7}
10.3	6.40
12.3	1.18×10^{-6}
12.6	1.33
12.9	1.35
13.2	1.69
13.6	2.18
14.0	2.64
16.4	2.80
16.5	2.98
19.0	4.50
19.6	5.17
20.2	5.53
20.6	6.17
26.0	1.52×10^{-5}
26.6	1.71
34.2	6.03
45.4	1.01×10^{-4}
64.4	3.52
67.0	6.20

Table A5
Steel: AOM-H1050
Specimen No.: U46-WR5
R: 0.80

ΔK (ksi$\sqrt{\text{in.}}$)	da/dN (in./cycle)
10.2	7.55×10^{-7}
11.3	1.15×10^{-6}
11.6	1.23
11.8	1.41
12.0	1.53
12.2	1.48
13.6	2.53
13.9	2.82
14.1	3.03
14.4	3.40
14.5	2.75
15.7	4.50
15.9	5.85
16.1	5.95
16.3	6.10
16.5	6.35
16.7	7.00
16.9	6.65
17.1	7.53
18.7	9.62
18.9	1.08×10^{-5}
19.2	1.02
19.4	1.26
19.9	1.16
21.5	1.77
21.8	1.90
22.0	2.08
22.2	2.10
22.4	2.00
22.6	2.30
22.9	2.18
23.1	2.10
23.4	2.58
25.2	2.50
25.5	3.30
25.8	3.38
26.1	2.95
26.4	3.10
26.7	3.08
27.1	3.88
29.5	5.30
30.0	4.67
30.3	5.50
30.6	5.15
31.0	5.95
31.3	6.60
33.5	1.27×10^{-4}
33.9	1.17
34.3	1.37
34.8	1.49
35.2	1.17
35.7	1.80

Table A6
Steel: AOM-H1150
Specimen No.: U46-WR7
R: 0.04

ΔK (ksi$\sqrt{\text{in.}}$)	da/dN (in./cycle)
31.0	8.82×10^{-6}
33.9	9.34
37.9	1.03×10^{-5}
46.9	1.56
51.4	1.92
55.3	2.36
62.0	2.95
69.8	4.07
75.1	5.33
80.3	6.43
86.8	7.99
101	1.41×10^{-4}
109	2.43
119	2.76
127	5.11
135	6.87

Table A7
Steel: AOM-H1150
Specimen No.: U46-WR9
R = 0.05

ΔK (ksi$\sqrt{\text{in.}}$)	da/dN (in./cycle)
13.5	4.43×10^{-7}
13.9	4.88
14.3	4.88
20.2	1.44×10^{-6}
20.7	1.55
21.1	1.53
27.4	2.95
27.9	3.08
28.4	3.35
29.5	3.46
30.1	5.48
32.2	6.17
46.9	9.75
49.1	1.00×10^{-5}
49.9	1.18
74.6	4.40
75.8	6.83
89.2	1.82×10^{-4}
90.6	1.46
114	5.33

Table A8
Steel: AOM-H1150
Specimen No.: U46-WR8
R: 0.67

ΔK (ksi$\sqrt{\text{in.}}$)	da/dN (in./cycle)
10.5	4.15×10^{-7}
12.4	8.05
12.7	8.85
12.9	9.65
13.2	1.05×10^{-6}
13.5	1.21
16.1	2.00
16.5	2.30
19.5	3.60
20.3	4.18
21.0	4.33
26.2	8.36
26.7	9.70
27.7	1.10×10^{-5}
33.6	2.46
34.4	2.35
34.9	2.58
35.5	3.11
44.5	1.11×10^{-4}
53.6	2.44
54.4	3.08
55.6	3.62

Table A9
Steel: AOM-H1150
Specimen No.: U46-WR10
R: 0.67

ΔK (ksi$\sqrt{\text{in.}}$)	da/dN (in./cycle)
22.1	7.00×10^{-6}
28.6	1.71×10^{-5}
29.3	1.53
30.0	2.02
36.9	4.68
37.6	5.53
56.7	3.28×10^{-4}
58.3	2.74

Table A10
Steel: AOM-H1150
Specimen No.: U46-WR11
R: 0.80

ΔK (ksi$\sqrt{\text{in.}}$)	da/dN (in./cycle)
11.0	7.35×10^{-7}
11.2	7.60
11.3	7.27
11.5	8.53
11.6	7.80
11.8	9.27
12.0	9.80
13.3	1.45×10^{-6}
13.6	1.58
13.8	1.50
14.0	1.71
14.3	1.73
15.7	2.34
15.9	2.62
16.1	2.40
16.3	2.56
16.6	3.20
16.8	2.88
18.3	4.53
18.5	3.90
18.7	4.23
19.0	4.63
19.2	4.93
19.5	5.00
21.2	7.10
21.5	9.00
21.8	9.13
22.1	8.87
22.4	1.01×10^{-5}
22.7	1.17
24.7	1.28
25.0	1.60
25.4	2.03
25.8	1.98
26.0	2.02
26.3	1.88
28.2	2.78
28.5	2.73
28.7	2.45
29.0	1.90
29.2	2.33
29.5	2.05
34.7	6.17

Table A11
Steel: VM-H1050
Specimen No.: U69-F3
R: 0.04

ΔK (ksi$\sqrt{\text{in.}}$)	da/dN (in./cycle)
10.2	3.93×10^{-7}
10.5	4.20
11.1	4.73
11.4	5.15
11.7	5.63
12.0	6.03
12.2	6.18
12.5	6.84
12.7	7.28
13.0	7.74
13.3	8.24
13.9	9.41
14.2	1.12×10^{-6}
16.9	1.90
17.1	1.75
17.3	1.93
17.8	2.08
22.7	3.73
23.3	4.00
23.9	4.42
30.1	7.42
37.5	1.08×10^{-5}
38.3	1.31
67.2	5.03
68.2	4.10

Table A12
Steel: VM-H1050
Specimen No.: U69-F1
R: 0.04

ΔK (ksi$\sqrt{\text{in.}}$)	da/dN (in./cycle)
17.8	2.37×10^{-6}
19.4	2.82
20.4	3.16
21.3	3.54
22.2	3.54
23.2	4.10
24.1	4.35
25.0	4.79
26.4	5.16
28.0	5.90
29.1	6.46
29.9	7.22
30.8	7.19
32.0	8.44
33.1	8.88
34.4	8.73
36.2	8.69
38.5	1.25×10^{-5}
41.2	1.28
44.2	1.57
47.2	1.58
50.5	2.10
54.0	2.46
56.4	2.41
59.2	3.12
63.0	3.20
67.1	3.69
71.5	4.17
77.1	4.97
82.6	6.31
87.5	7.29
93.5	9.20
99.3	8.80
105	1.17×10^{-4}
113	1.45
125	1.74
163	4.04

Table A13
Steel: VM-H1050
Specimen No.: U69-F5
R: 0.40

ΔK (ksi$\sqrt{\text{in.}}$)	da/dN (in./cycle)
12.0	1.04×10^{-6}
12.2	1.17
12.5	1.24
15.8	2.59
16.1	2.61
16.4	2.72
16.7	2.82
16.9	3.20
23.5	6.10
24.0	6.53
24.3	6.30
24.7	7.00
24.9	5.90
32.2	1.23×10^{-5}
32.8	1.21
33.3	1.33
33.9	1.40
42.5	2.00
43.2	2.80
43.8	2.30
44.4	2.63
45.1	2.32
54.4	4.60
55.0	4.13
56.3	4.63
57.0	5.00
57.9	5.77
68.4	1.00×10^{-4}
69.2	9.40×10^{-5}
70.4	1.16×10^{-4}
71.5	1.56
82.7	1.74
83.5	2.42
84.9	2.28
87.9	2.35
101	6.50
104	6.28
111	5.70
121	6.26

Table A14
Steel: VM-H1050
Specimen No.: U69-F2
R: 0.67

ΔK (ksi$\sqrt{\text{in.}}$)	da/dN (in./cycle)
14.4	1.8×10^{-6}
15.0	2.23
15.6	2.29
16.2	2.60
16.9	2.84
17.6	3.19
18.3	3.03
19.0	3.40
19.8	4.16
21.0	4.60
22.2	4.85
23.1	5.48
24.2	6.07
25.6	7.34
27.3	8.09
28.6	8.67
29.7	9.29
31.5	1.11×10^{-5}
33.4	1.21
35.3	1.42
37.4	1.76
39.7	2.13
42.1	2.48
43.8	2.99
45.7	3.66
48.8	5.61
52.6	6.37
56.6	8.52
60.2	1.05×10^{-4}
62.7	1.96
66.6	1.86
71.8	3.38
76.4	9.30
80.3	7.15

Table A15
Steel: VM-H1050
Specimen No.: U69-F6
R: 0.80

ΔK (ksi$\sqrt{\text{in.}}$)	da/dN (in./cycle)
10.2	9.65×10^{-7}
11.3	1.39×10^{-6}
12.1	1.68
13.4	2.06
13.9	2.46
15.5	2.82
15.7	2.67
16.0	3.05
16.5	2.93
18.2	4.78
18.7	4.28
19.0	4.50
20.7	5.10
21.0	5.67
21.7	6.07
22.0	6.27
23.8	7.15
24.1	7.80
24.5	8.10
24.9	9.40
25.3	1.02×10^{-5}
25.8	9.70×10^{-6}
27.9	1.40×10^{-5}
28.3	1.33
28.7	1.44
29.2	1.48
31.5	1.82
32.6	1.84
33.2	2.20
41.4	3.60